Supplementary Information

Using high-frequency oscillations from brief intraoperative neural recordings to predict the seizure onset.

Behrang Fazli Besheli[1], Zhiyi Sha[2], Jay R. Gavvala[3], Sacit Karamursel[4], Michael Quach[5], Chandra Prakash Swamy[1], Amir Hossein Ayyoubi[1], Alica M. Goldman[6], Daniel J. Curry[7], Sameer A. Sheth[8], David Darrow[9], Kai J. Miller[1], David J. Francis[10], Gregory A. Worrell[11], Thomas R. Henry[2], and Nuri F. Ince[1,12*]

1 Department of Neurologic Surgery, Mayo Clinic; Rochester, MN, 55905 USA.
2 Department of Neurology, University of Minnesota; Minneapolis, MN 55401 USA.
3 Department of Neurology, UT Health; Houston, TX, 77030 USA.
4 Department of Physiology, School of Medicine, Koç Üniversitesi; Istanbul, Türkiye
5 Department of Neurology, Texas Children's Hospital; Houston, TX, 77030 USA.
6 Department of Neurology-Neurophysiology, Baylor College of Medicine; Houston, TX, 77030 USA.
7 Department of Neurosurgery, Texas Children's Hospital; Houston, TX, 77030 USA.
8 Department of Neurosurgery, Baylor College of Medicine; Houston, TX, 77030 USA.
9 Department of Neurosurgery, University of Minnesota; Minneapolis, MN, 55401 USA.
10 Department of Psychology, University of Houston; Houston, TX, 77030 USA.
11 Department of Neurology, Mayo Clinic; Rochester, MN 55905, USA.
12 Department of Biomedical Engineering, Mayo Clinic; Rochester, MN, 55905 USA.

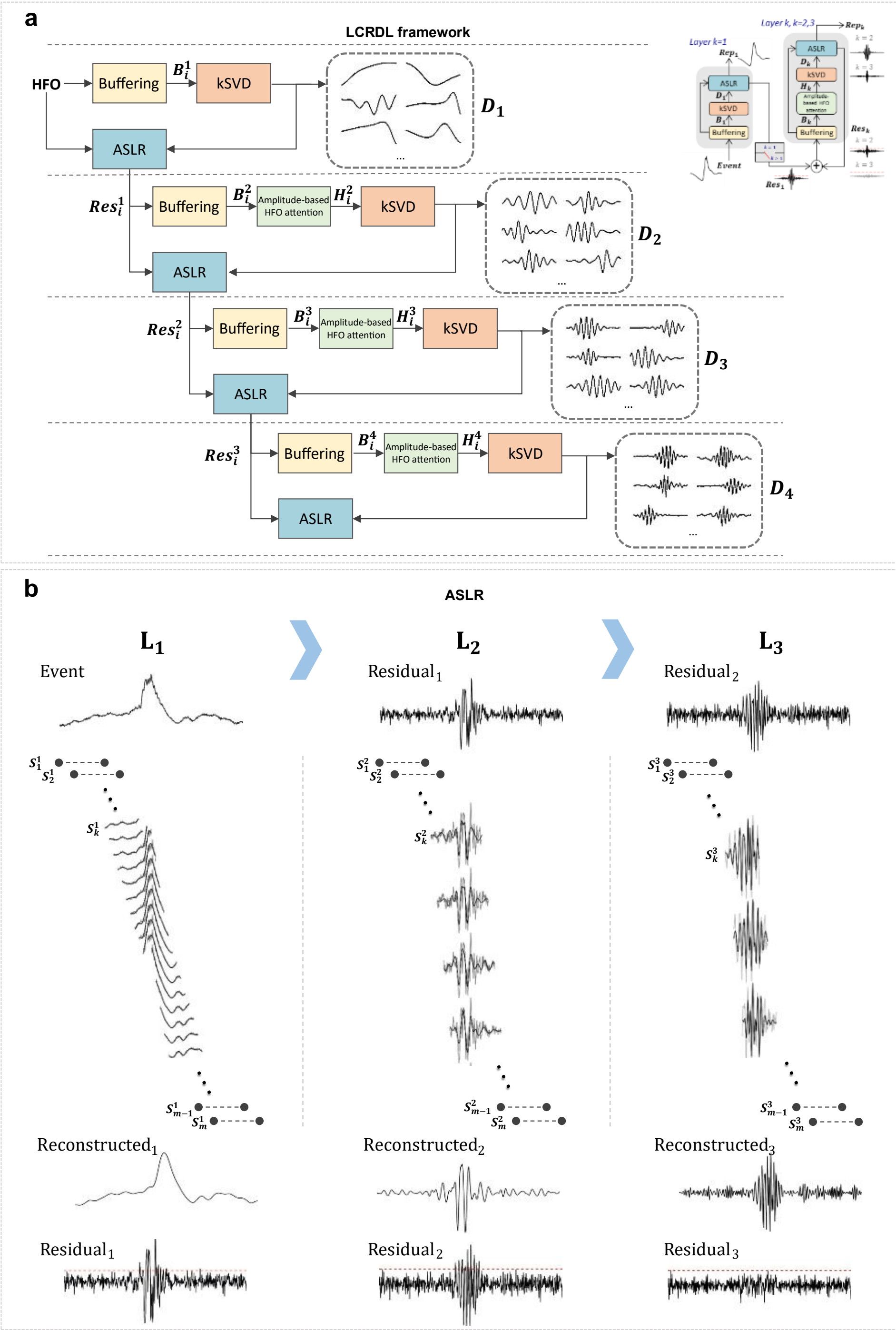

Supplementary Fig. S1. The schematic of LRCDL dictionary learning and ASLR representation. a The residual-based cascaded dictionary learning: all annotated HFOs are utilized to learn a local dictionary of atoms. The process begins with the segmentation of HFO events using a buffer function, which is then input into a kSVD dictionary learning algorithm to create the initial level of the dictionary. Utilizing this dictionary and the ASLR technique, all events are represented, and the residual signal is computed. Then, in the subsequent levels, the residual segments with high-frequency components that pass an amplitude detector are selected to establish the subsequent layers of the dictionary. In this scheme, we opted for four layers in the dictionary learning process because, after this layer, no HFO components exist for learning in the deeper layer. Additionally, as both the third and fourth layers contained HFO patterns above 250 Hz in the FR band, we merged them into one single dictionary for the representation phase, ultimately employing three layers for ASLR representation. **b** The ASLR method outlines a three-stage representation process employed to represent the events using local atoms. In the first stage, D_1 dictionaries are applied over a moving window to locally represent the event. In the second stage, the residual signal from the first stage representation is represented using a D_2 dictionary. Finally, in the third stage, the remaining residual is represented using D_3 and D_4 dictionaries. The overall representation of the event is obtained by summing up the representations from all three stages. LCRDL local cascaded residual-based dictionary learning, kSVD k-singular value decomposition, ASLR adaptive sparse local representation, HFO high-frequency oscillation.

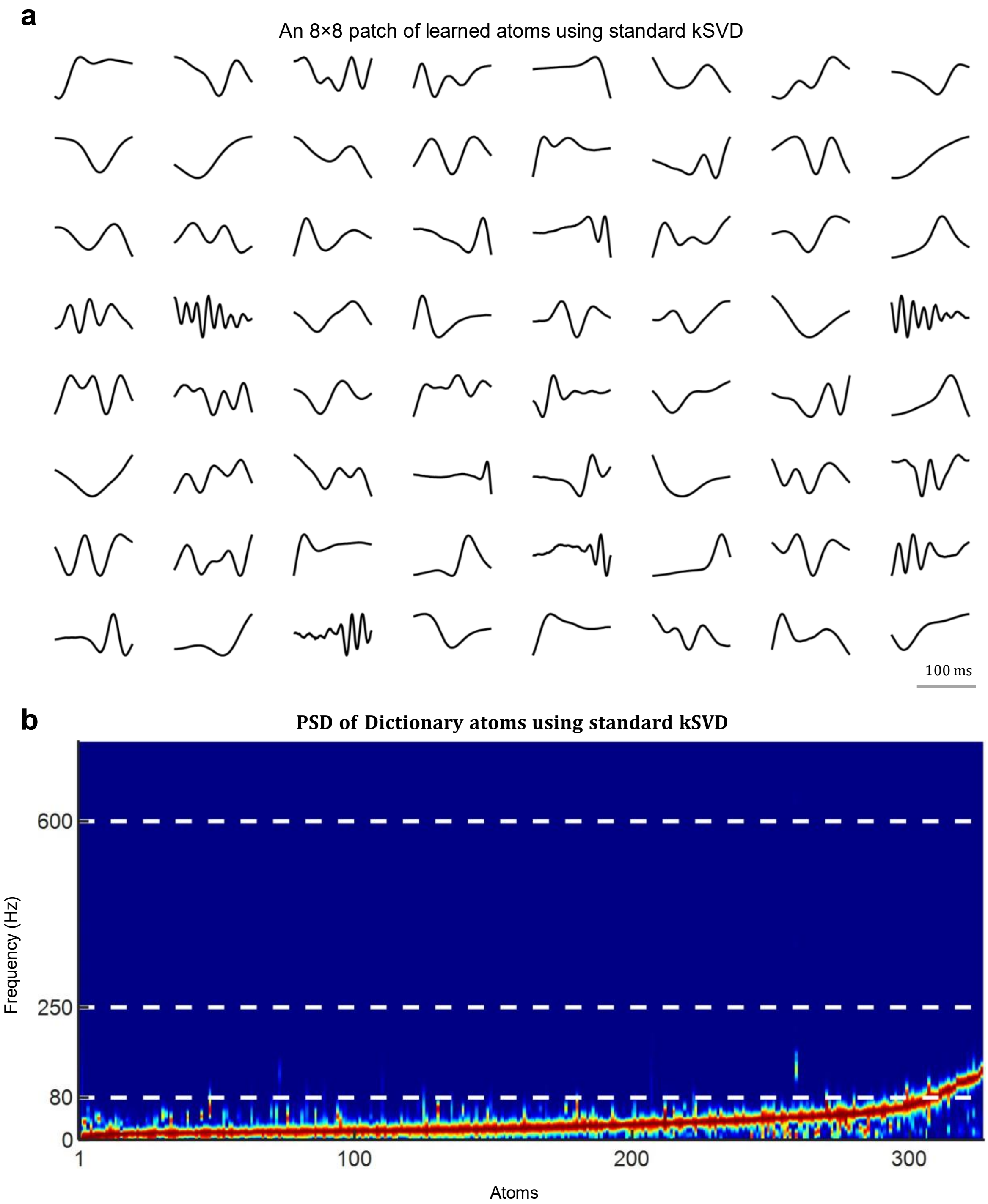

Supplementary Fig. S2. The learned atoms using general kSVD without cascaded residual-based learning. a It displays the learned dictionary atoms by applying the general kSVD. **b** The PSD of the D atoms. In a single-layer learning process, kSVD failed to capture HFO patterns above 120 Hz due to the energy difference between low and high-frequency electrophysiological data. kSVD K-singular value decomposition, PSD power spectral density.

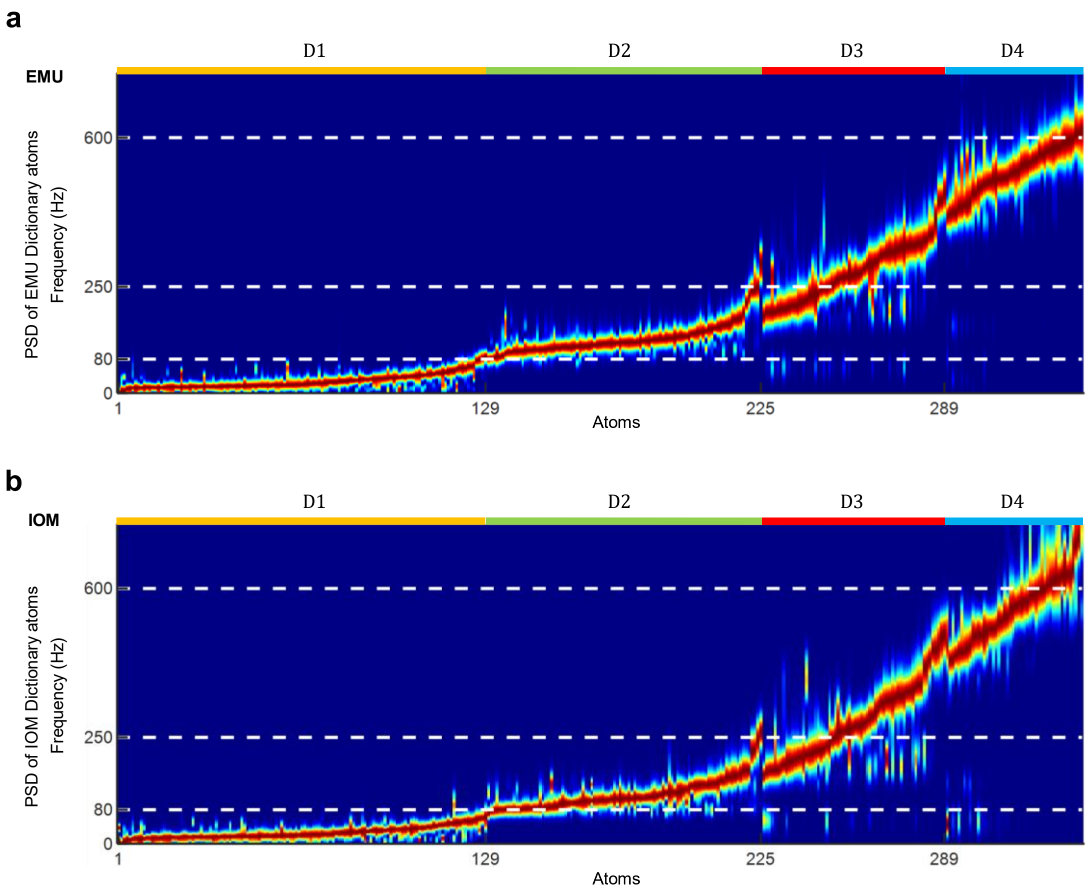

Supplementary Fig. S3. The PSD of all learned atoms. a EMU and **b** IOM scenarios. Across different layers (D_{1-4}), the shallow layers predominantly learned low-frequency atoms below 80 Hz, while the mid layers generated atoms within the R band. The deepest layer primarily produced atoms in the FR band. PSD power spectral density, IOM intraoperative monitoring, EMU epilepsy monitoring unit, R ripple, FR fast ripple.

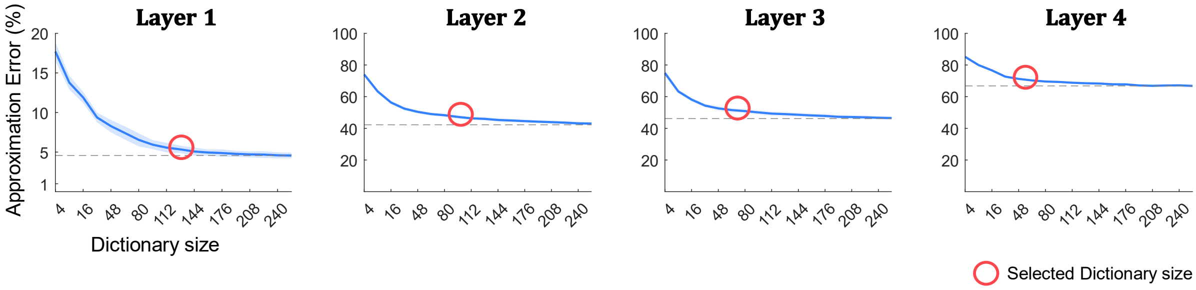

Supplementary Fig. S4. Dictionary size at each layer. The approximation error of HFOs is calculated using various dictionary sizes, and the smallest size providing an acceptable level of approximation is chosen for each layer. The dictionary size is selected to strike a balance between having compact dictionaries and achieving an acceptable approximation error for representing HFO events. Starting with the first layer for the coarsest representation, the size of local atoms was set to 64 ms. In subsequent layers, the size of local atoms was gradually reduced, resulting in a length of 64 ms for D_2, while both D_3 and D_4 had a length of 32 ms. Furthermore, we learned 128, 96, 64, and 48 atoms for D_1 to D_4, respectively.

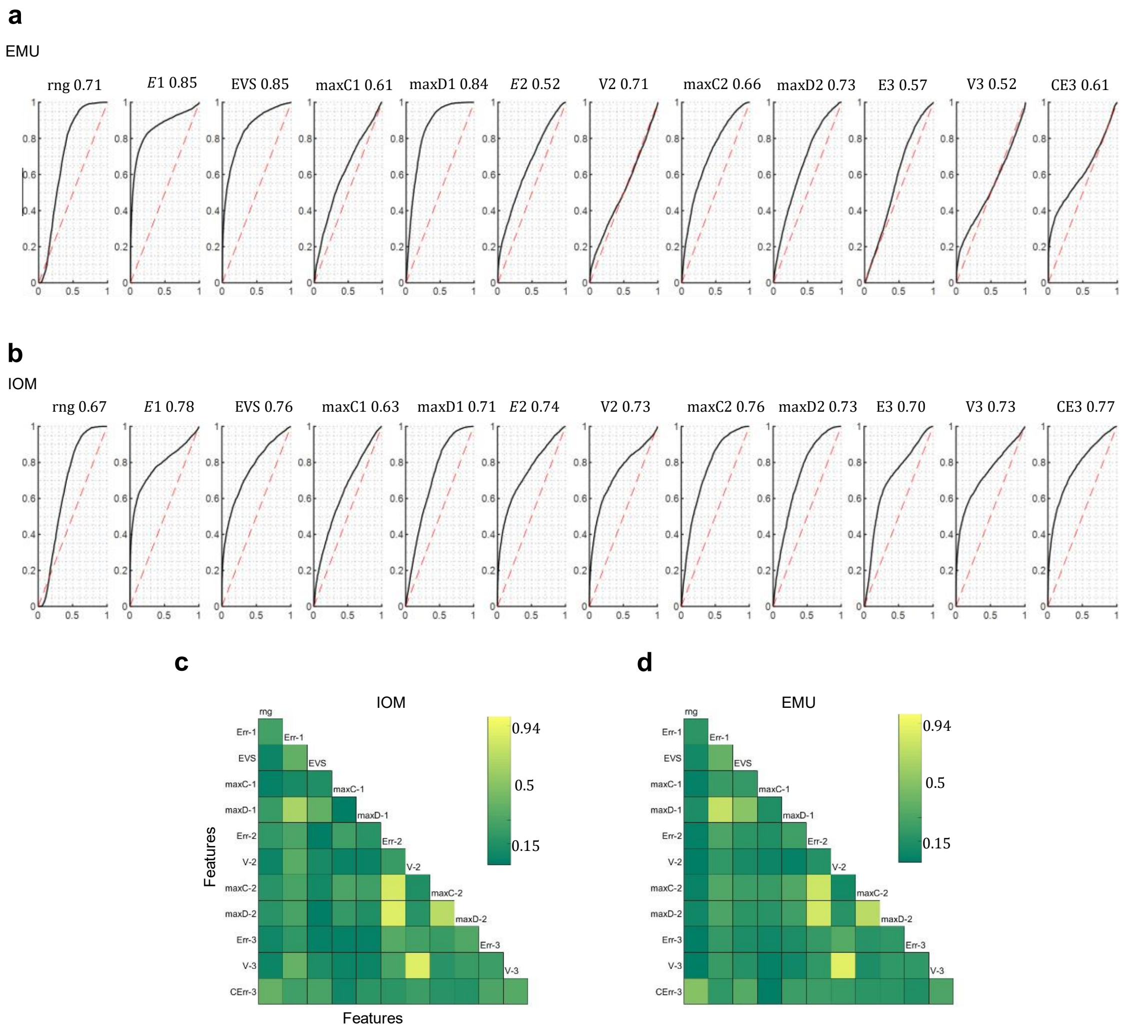

Scenario	Reconstruction type	Dictionary	Model	Data
I	L2-OMP	IOM	IOM	IOM
II	L2-OMP	EMU	IOM	IOM
III	L2-OMP	EMU	EMU	EMU
IV	L2-OMP	IOM	EMU	EMU
V	L2-OMP	EMU	EMU	IOM
VI	L2-OMP	IOM	IOM	EMU

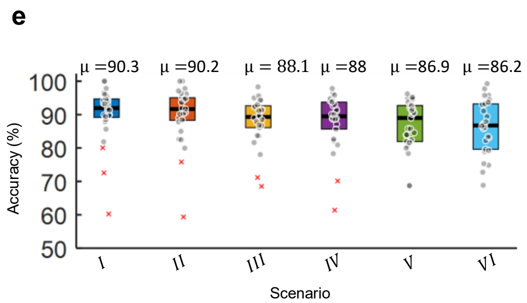

Supplementary Fig. S5. Extracted features and classification accuracy. a ROC curves and corresponding AUC values depicting the performance of extracted features from annotated EMU events. **b** ROC curves and corresponding AUC values depicting the performance of extracted features from annotated IOM events. **c, d** The correlation analysis of the extracted features between IOM and EMU annotated events. **e** Applying the dictionary and model learned from IOM/EMU to EMU/IOM annotated events. The statistical analysis revealed no significant differences when substituting the IOM and EMU dictionaries with each other. However, when we established the entire classifier using EMU data and applied it to IOM, a notable 3.4% reduction in the classification accuracy (from 90.3% to 86.9%, p=0.001) was observed. Conversely, when the model was generated from IOM data and applied to EMU, the decrease in classification accuracy was 1.9% (from 88.1% to 86.2%, p=0.001). Application of the IOM dictionary/model to EMU annotated data and vice versa. OMP orthogonal matching pursuit, IOM intraoperative monitoring, EMU epilepsy monitoring unit.

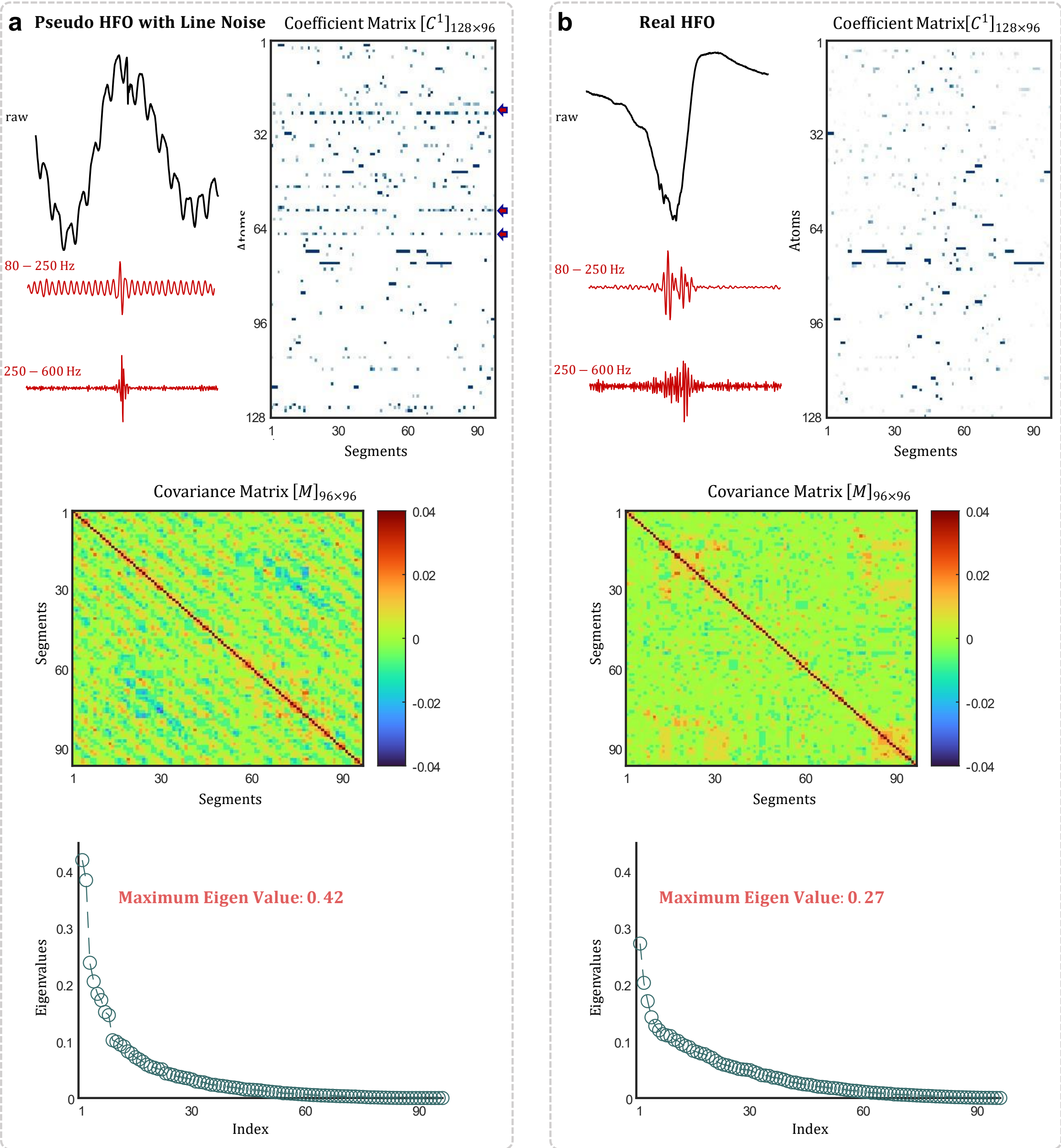

Supplementary Fig. S6. Coefficient matrix example of real and pseudo-HFO. a An example of a pseudo-HFO with a 60 Hz line noise and its harmonics. The corresponding trace in the R and FR bands are given. The covariance matrix (M) of the first layer of the coefficient matrix (C) is visualized with sorted eigenvalues. Due to the repetitive selection of a subset of atoms during representation over segments, the coefficient matrix exhibits high eigenvalues (0.42). **b** An example of real HFO, which, despite having structured waveforms, does not result in the spatial selection of a few atoms during ASLR representation. Consequently, the maximum eigenvalue of the coefficient matrix of the representation is small (0.27), distinguishing it from pseudo-HFOs with abnormal repetitive non-neural patterns.

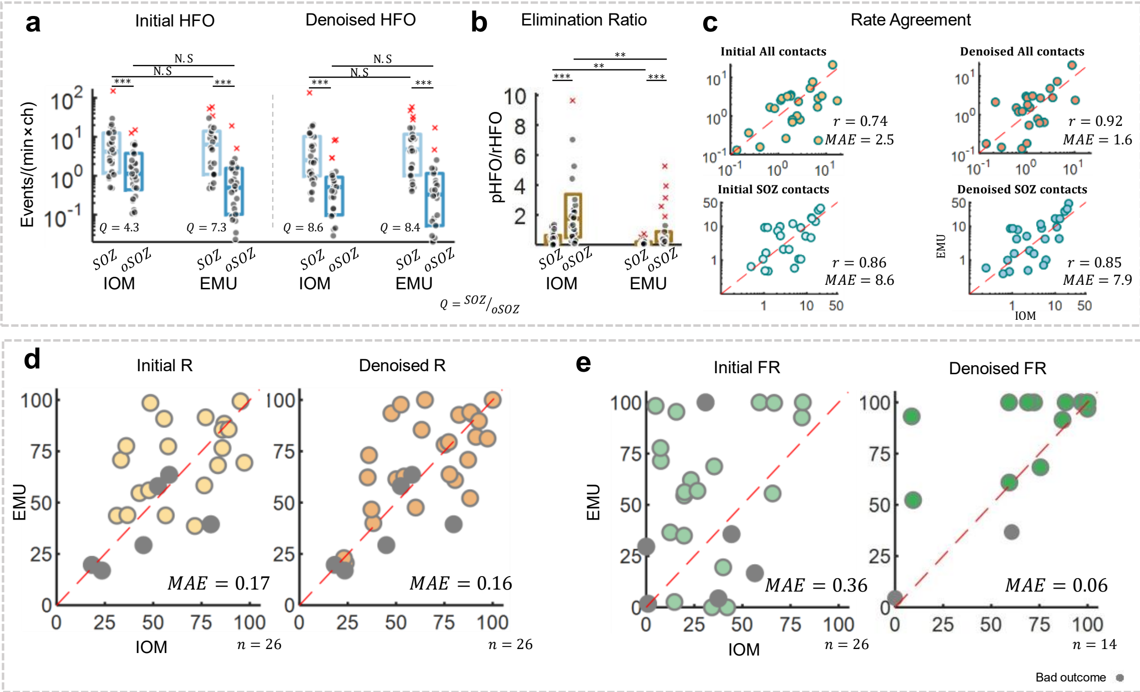

Supplementary Fig. S7. The agreement between HFO in IOM and EMU at the subject level. a Normalized rate of Events in iEEG recording across subjects (total rate in each subject divided by the duration and total number of contacts): The first panel shows the rate of events detected using the amplitude-threshold detector in and out of SOZ contacts across subjects (n^{IOM}=29, n^{EMU}=26). The Q-factor is calculated as Q=HFO^{SOZ}/HFO^{oSOZ}. The second panel shows the rate of real-HFOs passing the proposed method. **b** The elimination ratio, defined as the number of classified pseudo-HFOs to the real-HFOs, indicates more pseudo-HFOs were eliminated in the IOM compared to the EMU, particularly from oSOZ. **c** The agreement between the rates of HFOs detected in IOM and EMU before and after pseudo-HFO elimination. The rate of events prior to pseudo-HFO elimination across all contacts, compared to the post-elimination rate between recording scenarios, is more off-diagonal. **d, e** Comparison of percentages of Rs and FRs within the SOZ contacts before (Initial) and after (Denoised) pseudo-HFO elimination. The error bars represent the median with 25th and 75th percentiles. All values in this figure are presented as mean ± std. *r* represents the correlation coefficient between the x and y values of the agreement plot. IOM intraoperative monitoring, EMU epilepsy monitoring unit, HFO high-frequency oscillation, R ripple, FR fast ripple, SOZ seizure onset zone, oSOZ, out of seizure onset zone, MAE mean absolute error.

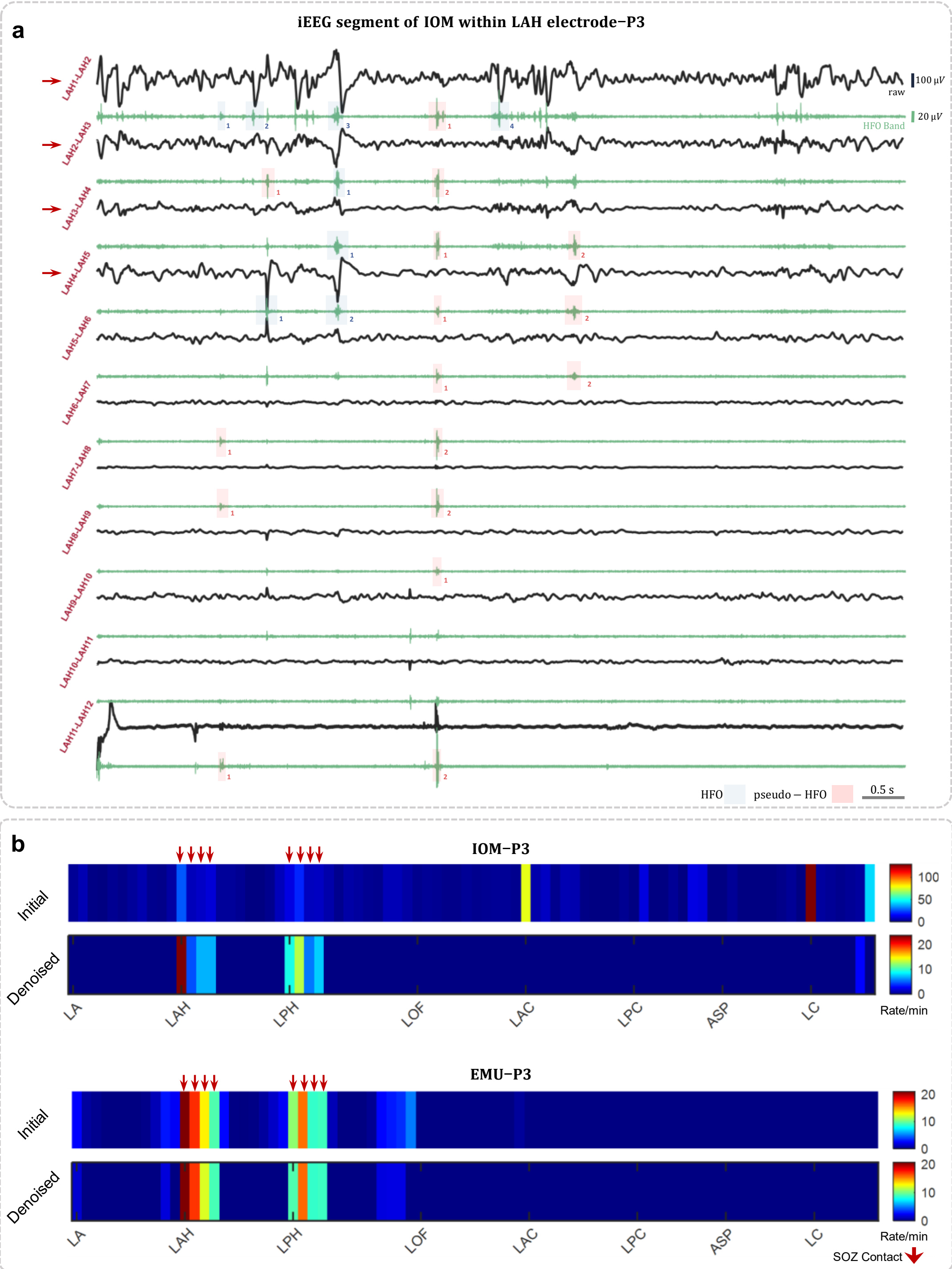

Supplementary Fig. S8. Distribution of HFO in a representative subject P3. a A 10-second raw iEEG data (black trace) and corresponding HFO-band data (green trace), along with the detected events in the LAH electrode of subject P3. **b** Heatmap of HFO distribution (rate per minute) for each contact in subject P3. The heatmaps represents the IOM and the EMU data, both before and after pseudo-HFO elimination. IOM intraoperative monitoring, EMU epilepsy monitoring unit, HFO high frequency oscillation, SOZ seizure onset zone, LA: Left Amygdala, LAH: Left Anterior Hippocampus, LPH: Left Posterior Hippocampus, LOF: Left Orbital Frontal, LAC: Left Anterior Cingulate, LPC: Left Posterior Cingulate, ASP: Left Anterior-superior Precuneus, LC: Left Anterior Cuneus.

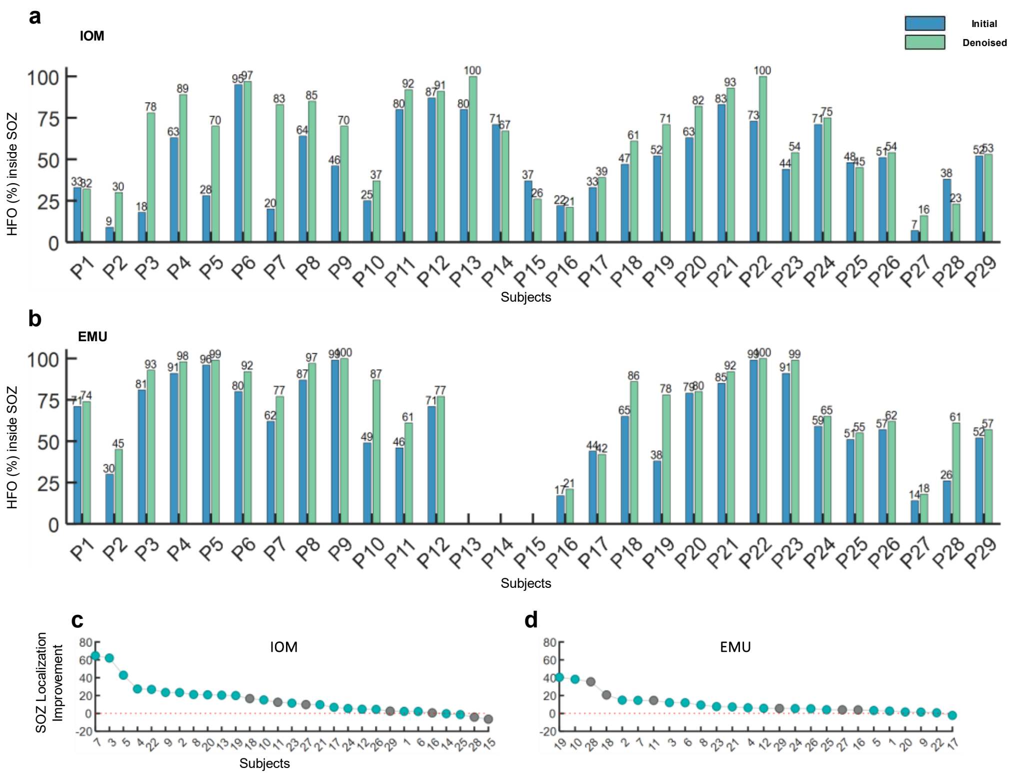

Supplementary Fig. S9. SOZ localization accuracy before and after pseudo-HFO elimination. a In IOM, **b** in EMU**. c, d** The improvements in SOZ localization accuracy in each subject. IOM intraoperative monitoring, EMU epilepsy monitoring unit, HFO high frequency oscillation, SOZ seizure onset zone.

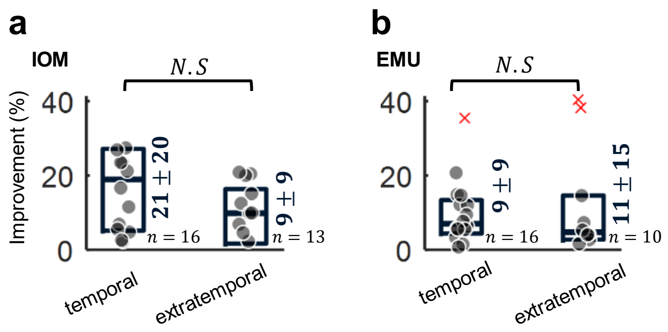

Supplementary Fig. S10. Comparison of SOZ localization improvement after pseudo-HFO elimination across anatomical regions for IOM and EMU recordings. a Improvement in SOZ delineation using IOM HFO spatial distribution after pseudo-HFO elimination (*p*=0.073) among temporal and extratemporal cases. Although the improvement in SOZ delineation was notably higher in temporal cases compared to extratemporal cases in IOM recordings, no significant difference is observed between these two groups. **b** The SOZ delineation improvement using EMU HFO spatial distribution after pseudo-HFO elimination (*p*=0.63) among temporal and extratemporal cases. The error bars represent the median with 25th and 75th percentiles. Outliers are shown as red ×. All values in this figure are presented as mean ± std. IOM intraoperative monitoring, EMU epilepsy monitoring unit. N.S. indicates that the p-value is above 0.05.

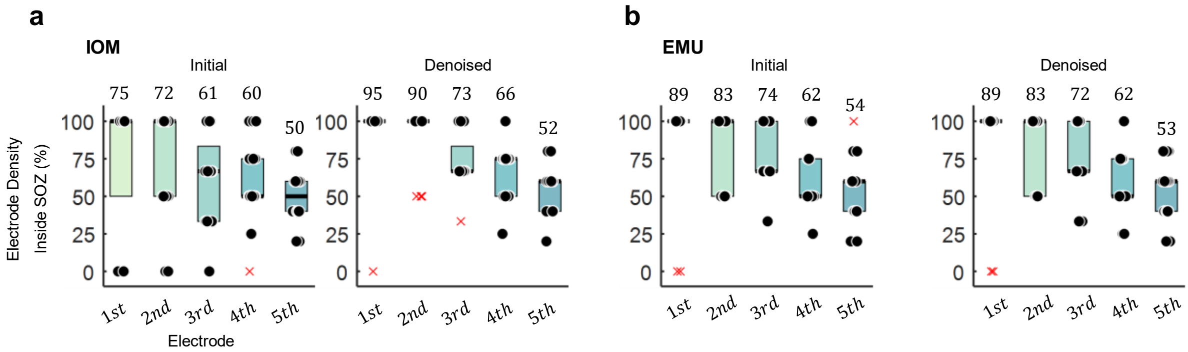

Supplementary Fig. S11. Electrode HFO density analysis. a, b The relationship between the first *k* electrodes with the highest HFO rate and clinically defined SOZ in IOM and EMU. As shown in this panel, 75% of electrodes with the highest rate of HFOs are in SOZ in the IOM scenario before the pseudo-HFO elimination compared to 95% after the pseudo-HFO elimination. This value decreased to 90%, 73%, 66%, and 52% for the first 2, 3, 4, and 5 electrodes after pseudo-HFO elimination. On the other side, 90%, 83%, 72%, 62%, and 53% were reported after pseudo-HFO elimination. Furthermore, no significant improvement was observed in EMU since the small amount of pseudo-HFOs in EMU could not change the density of electrodes. The error bars represent the median with 25th and 75th percentiles. All values in this figure are presented as mean ± std. Outliers are shown as red ×. IOM intraoperative monitoring, EMU epilepsy monitoring unit, SOZ seizure onset zone.

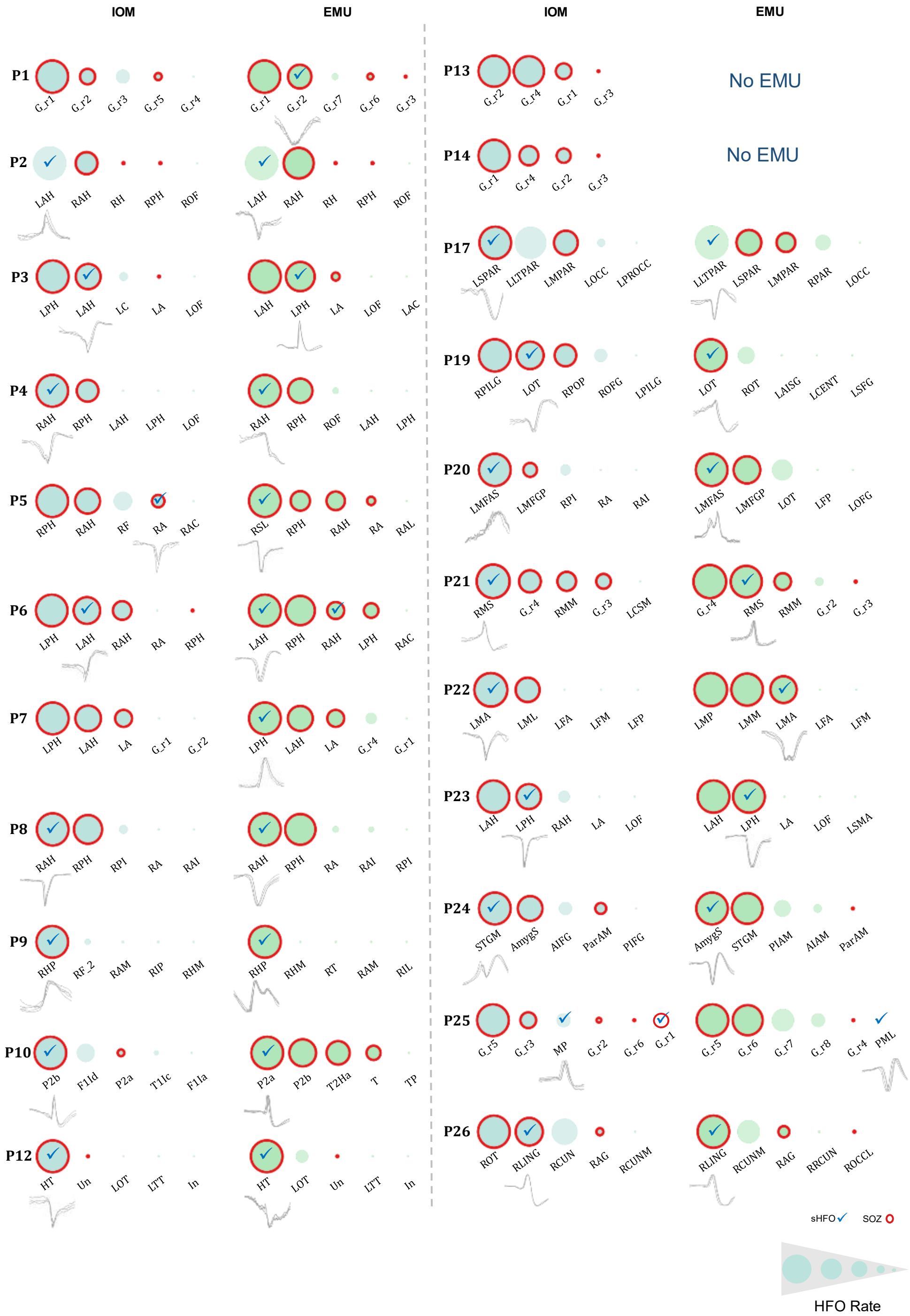

Supplementary Fig. S12. Comprehensive comparison of the HFO electrode density and sHFO. Electrodes are sorted based on the highest rate of detected HFOs, and sHFOs are marked with "✓" across all subjects in both IOM and EMU. Additionally, the SOZ electrodes are marked with red circles around each electrode. The detected sHFO events and their waveforms are also visualized below each plot. IOM intraoperative monitoring, EMU epilepsy monitoring unit, HFO high-frequency oscillation, SOZ seizure onset zone, sHFO stereotyped HFO. All electrode positions are mentioned in Supplementary Data 1.

Supplementary Table 1. Patient-level clinical validation of HFO region and surgical outcome

Subject	Predictive outcome of SOZ	Predictive outcome of detected events			
		IOM HFO		EMU HFO	
		Initial	Denoised	Initial	Denoised
P1-UM	TN	FP	TN	TN	TN
P2-UM	TN	FP	FP	FP	FP
P3-UM	TN	FP	TN	TN	TN
P4-UM	TN	TN	TN	TN	TN
P5-UM	TN	FP	TN	TN	TN
P7-UM	No resective surgery (RNS)	--	--	--	--
P8-UM	TN	TN	TN	TN	TN
P9-BCM	TN	TN	TN	TN	TN
P10-BCM	FP	FP	TN	FP	TN
P11-BCM	FN	FN	FN	FN	FN
P12-BCM	TN	TN	TN	TN	TN
P13-BCM	TN	TN	TN	No EMU	No EMU
P14-BCM	TN	FP	FP	No EMU	No EMU
P15-BCM	FN	TP	TP	No EMU	No EMU
P16-BCM	No resective surgery (VNS)	--	--	--	--
P17-BCM	TN	FP	FP	FP	FP
P18-BCM	TP	TP	TP	TP	TP
P19-BCM	TN	FP	FP	TN	TN
P20-BCM	TN	TN	TN	FP	FP
P21-UM	No resective surgery (RNS)	--	--	--	--
P22-UM	No resective surgery (RNS)	--	--	--	--
P23-UM	TN	FP	TN	TN	TN
P24-BCM	TN	TN	TN	TN	TN
P25-BCM	TN	FP	FP	FP	FP
P26-BCM	No resective surgery (RNS)	--	--	--	--
P27-BCM	FN	TP	TP	TP	TP
P28-BCM	TN	FP	FP	FP	TN
P29-BCM	TN	FP	FP	TN	TN
NPV	**0.85 (95% CI [0.64 0.97])**	**0.87 (95% CI [0.47 1.00])**	**0.92 (95% CI [0.64 1.00])**	**0.91 (95% CI [0.62 1.00])**	**0.93 (95% CI [0.66 1.00])**
PPV	**0.5 (95% CI [0.01 0.99])**	**0.2 (95% CI [0.04 0.48])**	**0.3 (95% CI [0.07 0.65])**	**0.25 (95% CI [0.03 0.65])**	**0.33 (95% CI [0.04 1.00])**

Supplementary Table 2. Computational time*

Method		Average Processing Time (ms per Event)
Initial detection	Amplitude threshold detection	9 ms/Event
Classification	Step 1. Feature extraction	108 ms/Event
	Step 2. Prediction	<1 ms/Event
Total		**~117 ms/Event**

* **Hardware:** Intel(R) Xeon(R) w9-3475X 2.21 GHz, 512 GB installed RAM, **Environment:** MATLAB 2022b, MATHWORKS, Natick/USA